

Phase diagrams and magnetic properties of the mixed spin-1 and spin-3/2 Ising ferromagnetic thin film: Monte Carlo treatment

B Boughazi, M Boughrara, M Kerouad

Citation: Chin. Phys. B . 2019, 28(2): 027501. **doi:** 10.1088/1674-1056/28/2/027501
Journal homepage: http://cpb.iphy.ac.cn; http://iopscience.iop.org/cpb

What follows is a list of articles you may be interested in

Effect of particle size distribution on magnetic behavior of nanoparticles with uniaxial anisotropy

S Rizwan Ali, Farah Naz, Humaira Akber, M Naeem, S Imran Ali, S Abdul Basit, M Sarim, Sadaf Qaseem

Chin. Phys. B . 2018, 27(9): 097503. **doi:** 10.1088/1674-1056/27/9/097503

Typicality at quantum-critical points

Lu Liu(刘录), Anders W Sandvik, Wenan Guo(郭文安)

Chin. Phys. B . 2018, 27(8): 087501. **doi:** 10.1088/1674-1056/27/8/087501

Effect of exchange interaction in ferromagnetic superlattices: A Monte Carlo study

R Masrour, A Jabar

Chin. Phys. B . 2016, 25(10): 107502. **doi:** 10.1088/1674-1056/25/10/107502

Magnetocaloric and magnetic properties of La_2NiMnO_6 double perovskite

Masrour R, Jabar A

Chin. Phys. B . 2016, 25(8): 087502. **doi:** 10.1088/1674-1056/25/8/087502

Quantitative calculations of polarizations arising from the symmetric and antisymmetric exchange strictions in Tm-doped $GdMnO_3$

Qin Ming-Hui, Lin Lin, Li Lin, Jia Xing-Tao, Liu Jun-Ming

Chin. Phys. B . 2015, 24(3): 037509. **doi:** 10.1088/1674-1056/24/3/037509

Phase diagrams and magnetic properties of the mixed spin-1 and spin-3/2 Ising ferromagnetic thin film: Monte Carlo treatment

B Boughazi†, M Boughrara, and M Kerouad

Laboratoire Physique des Matériaux et Modélisation des Systémes (LP2MS), Unité Associée au CNRST-URAC: 08, *Faculty of Sciences, University Moulay Ismail, B P* 11201, *Zitoune, Meknes, Morocco*

(Received 12 June 2018; revised manuscript received 26 November 2018; published online 10 January 2019)

Phase diagrams and magnetic properties of the mixed spin-1 and spin-3/2 Ising film with different single-ion anisotropies are investigated, by the use of Monte Carlo simulation based on heat bath algorithms. The effects of the crystal-fields and the surface coupling on the phase diagrams are investigated in detail and the obtained phase diagrams are presented. Depending on the Hamiltonian parameters, the system exhibits both second- and first-order phase transitions besides tricritical point, triple point, and isolated critical end point.

Keywords: Monte Carlo simulation, thin film, phase diagrams, magnetic properties

PACS: 75.70.–i, 75.40.Mg, 75.70.Rf, 75.10.Hk **DOI:** 10.1088/1674-1056/28/2/027501

1. Introduction

Nowadays, the study of Ising thin films has received much attention experimentally and theoretically, because of the progress of the thin film deposition techniques[1–5] and for reasons ranging from fundamental investigations of phase transitions to technical problems encountered in thin film magnets.[6] From the theoretical point of view, many approximations have been used to study the magnetic properties of thin films, such as the mean-field approximation[7,8] and the effective-field theory with correlations.[9–16] Although each method has its own advantages, they all have limitations in treating film systems. Numerical techniques such as the Monte Carlo method[17–19] can provide very accurate results for properties of finite systems.

Critical phenomena and universality behavior of ferromagnetic thin films described by a spin-1 Blume–Capel Hamiltonian has been examined for various thickness values ranging from 3 to 40 layers.[20] When the surface exchange coupling is greater than a critical value, the surface region can exhibit an ordered phase even if the bulk is paramagnetic and it has a transition temperature higher than the bulk one. This fact has also been experimentally observed.[21–23] Boughrara *et al.* have applied Monte Carlo simulation to study the magnetic properties and the phase diagrams of a ferromagnetic thin film described by a Blume–Capel Hamiltonian in the presence of disordered crystal field interactions.[24] The authors have found that the system presents tricritical points which are observed at a certain interval of the crystal field and for lower values of the probability p which represents the disorder parameter. They have also shown that the randomness parameter p destroys the tricritical behavior and that the system exhibits reentrant and double reentrant behaviors for a certain range of p and D.

One of the well-known and most studied mixed spin Ising systems is the mixed spin-1 and spin-3/2 Ising system. From the experimental point of view, Stanica *et al.* synthesized quasi-one-dimensional heterotrinuclear complex $[NiCr_2(bipy)_2\ (C_2O_4)_4(H_2O)]H_2O$, that shows a rare case[25] of antiferromagnetism between Ni(II) $S = 1$ and Cr(III) $S = 3/2$. Theoretically, the mixed spin-1 and spin-3/2 Ising model have been studied by using a wide variety of methods in equilibrium statistical physics. Abubrig *et al.*,[26] performed a mean-field study in view of determining the effects of different crystal-fields on the phase diagrams of the mixed (spin-1 and spin-3/2) Ising system as well as the T-dependence of the total and sublattice magnetizations. By the use of mean field theory,[27] Souza *et al.* have explored the phase diagrams of a mixed spin-1 and spin-3/2 Ising model. The authors have shown that the phase diagrams exhibit the tricritical behavior, the first and the second-order phase transitions.

In this work, we are going to study, via Monte Carlo simulation, the surface effect and the influence of the crystal fields on the phase diagrams and the magnetic properties of a mixed spin (1,3/2) ferromagnetic thin film. The outline of this paper is as follows: in Section 2, we describe the model and we give the details of the Monte Carlo simulation. In Section 3, we present our results and discuss important points. Finally, the last section is devoted to a brief conclusion.

2. Model and formalism

We consider a ferromagnetic thin film with a simple cubic lattice containing up to L_z monolayers (Fig. 1(a)). In the

†Corresponding author. E-mail: brahim.boughazi@gmail.com

© 2019 Chinese Physical Society and IOP Publishing Ltd

Monte Carlo simulations based on the heat bath algorithm,[28] we apply periodic boundary conditions in the x and y directions and free boundary conditions in the z direction which is of finite thickness L_z. The Hamiltonian of the system is given by

$$H = -\sum_{\langle ij \rangle} JS_i\sigma_j - D_A\sum_{\langle i \rangle} S_i^2 - D_B\sum_{\langle j \rangle}\sigma_j^2, \tag{1}$$

where $S_i = \pm 3/2, \pm 1/2$, $\sigma_j = \pm 1, 0$ are the usual Ising variables, the summation is carried out only over nearest-neighbor pairs of spins and $J = J_S$ if the lattice sites i and j belong to one of the two surfaces of the film; otherwise, we take $J = J_1$, where J_S and J_1 denote the ferromagnetic surface and bulk exchange interactions, respectively (Fig. 1(b)). The first term in Eq. (1) is a summation over the nearest-neighbor spins, the second term represents the crystal field energy on the S-spins and the third term represents the crystal field energy on the σ-spins. For simplicity all system parameters are normalized by J_1. So that, $R_S = J_S/J_1$.

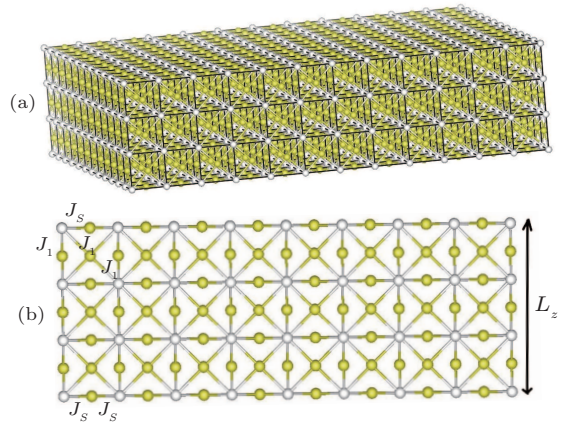


Fig. 1. (a) Schematic representation of a ferromagnetic thin film composed of L_z distinct monolayers. The bottom and top surfaces have monolayer thickness. Surface spin–spin interaction is denoted by J_S. Bulk region thickness is $L_z - 2$ with exchange coupling J_1. (b) A cross section of a ferromagnetic thin film consisting of two magnetic atoms A (white points with $S = 3/2$) and B (yellow points with $\sigma = 1$).

The simulations are carried out for face centered cubic film containing $N_T = N_x \times N_y \times L_z$ spins. $N_x \times N_y$ represents the number of sites in each layer of the film and L_z is the number of layers in it or its thickness. Results are reported for systems of size $N_x = N_y = 80$ and $L_z = 6$. A number of additional simulations were performed for $N_x = N_y = 40$, 60, 80, and 100 but no significant differences were found for $N_x = N_y \geq 80$. In our study, 4×10^4 Monte Carlo steps were used to obtain each data point in the system, after discarding the first 2×10^4 steps. The magnetization M of a configuration is defined by the sum over all the spin values of the lattice sites.

When studying the film properties, by employing the Monte Carlo simulation, we compute different physical quantities including the magnetizations per site of sublattices:

$$M_A = \frac{1}{N_A}\sum_{i=1}^{N_A}\langle S_i \rangle, \tag{2}$$

$$M_B = \frac{1}{N_B}\sum_{j=1}^{N_B}\langle \sigma_j \rangle. \tag{3}$$

The total magnetization per site which is given by

$$M_T = \langle M_i \rangle = \frac{1}{N_T}(N_A M_A + N_B M_B), \tag{4}$$

where M_i is the total magnetization for each configuration. N_A and N_B are the numbers of spin-3/2 and spin-1 respectively.

The total susceptibility of the film is defined as

$$\chi_T = \beta N_T(\langle M_T^2 \rangle - \langle M_T \rangle^2) \tag{5}$$

with $\beta = 1/K_B T$, K_B is the Boltzmann constant.

The total internal energy of the film is computed as

$$E_T = \frac{\langle H \rangle}{N_T}. \tag{6}$$

The critical temperatures are determined from the maxima of the susceptibility curves and the first-order phase transitions are obtained by locating the discontinuities of the magnetization and the internal energy curves.

3. Results and discussions

In this section, we examine the phase diagrams and the magnetic properties of the system for some selected values of the Hamiltonian parameters. The phase diagrams are examined only for the ferromagnetic case ($J > 0$). In all phase diagrams, lines with black circles and white circles are used to indicate the second- and first-order phase transitions, respectively, while large black stars and white stars represent the positions of tricritical and isolated critical points, respectively. The black square shows the position of the triple point.

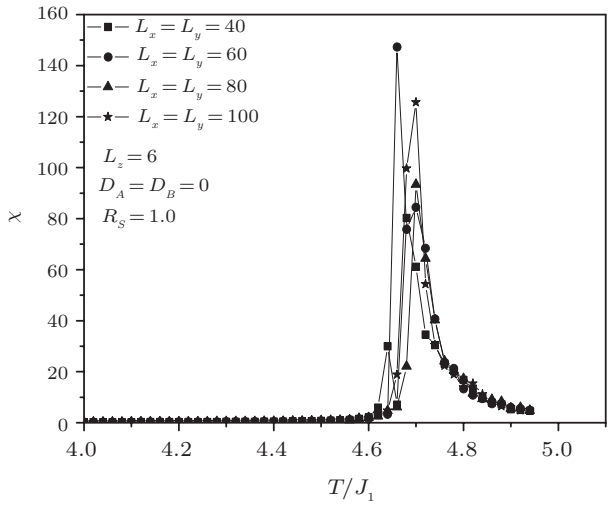


Fig. 2. The susceptibility versus T/J_1 for $R_S = 1.0$, $D_A/J_1 = D_B/J_1 = 0.0$, $L_z = 6$ and for different lengths of the wire.

In order to investigate the finite size effect on the magnetic properties of the system, we have plotted the susceptibility as a function of the temperature for $R_S = 1.0$, $D_A/J_1 = D_B/J_1 = 0.0$, $L_z = 6$ and for different sizes of the film ($L_x = L_y = 40$, 60, 80, and 100) (Fig. 2). We can see from these curves, that the value of the critical temperature is independent of the size of the system when $L_x = L_y \geq 80$. The variation of the Curie temperature T_C/J_1 with the thickness L_z of the film is shown in Fig. 3.

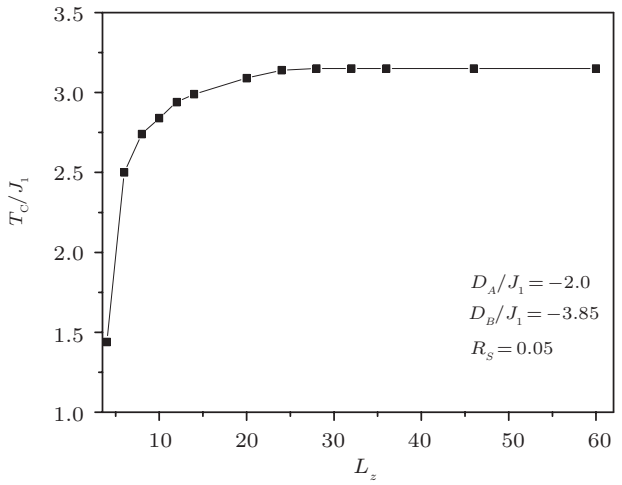


Fig. 3. The variation of the Curie temperature T_C/J_1 with the thickness (L_z) of the film for $D_A/J_1 = -2.0$, $D_B/J_1 = -3.85$, and $R_S = 0.05$.

As can be seen in this figure, a significant increase in T_C/J_1 can be detected when the thickness of the film is increased from $L_z = 4$ to $L_z = 24$. For $L_z = 24$, $T_C/J_1 = 3.14$ which is comparable to that of the bulk[29,30] and no obvious changes can be observed in T_C/J_1 when the thickness of the film is further increased to $L_z = 60$. Hence, we can conclude that, for $L_z \geq 24$, the magnetic properties of the mixed spin-1 and spin-3/2 Ising film are comparable to those of the bulk.

The phase diagrams in the $(T_C/J_1, R_S)$ plane for $D_B/J_1 = -3.85$ and for different values of D_A/J_1 are plotted in Fig. 4. As can be seen, depending on the value of D_A/J_1, we can have four types of phase diagrams. The first one, obtained for $D_A/J_1 \leq -4.45$, is presented in Fig. 4(a) for $D_A/J_1 = -6.0$. It is observed that the system exhibits two types of transition lines separating the ordered and disordered phases, the first one is a first-order transition line which starts from $R_S = 1.95$ at $T_C/J_1 = 0.0$ and increases with increasing R_S to terminate at a tricritical point. The second one is a second-order transition line, which extends from the tricritical point and increases with increasing (R_S) to reach a saturation value ($T_{Csat}/J_1 = 1.82$ for $R_S \geq 6.0$). The second type of phase diagram, obtained for $-4.45 < D_A/J_1 < -3.10$, is plotted in Fig. 4(b) for $D_A/J_1 = -3.5$, in this phase diagram we have three ordered phases (O_1, O_2, and O_3) and a disordered one (P) separated by three transition lines. In the low temperature region, a first-order transition line emerges from $R_S = 0.95$ at $T_C/J_1 = 0.0$, separates the two

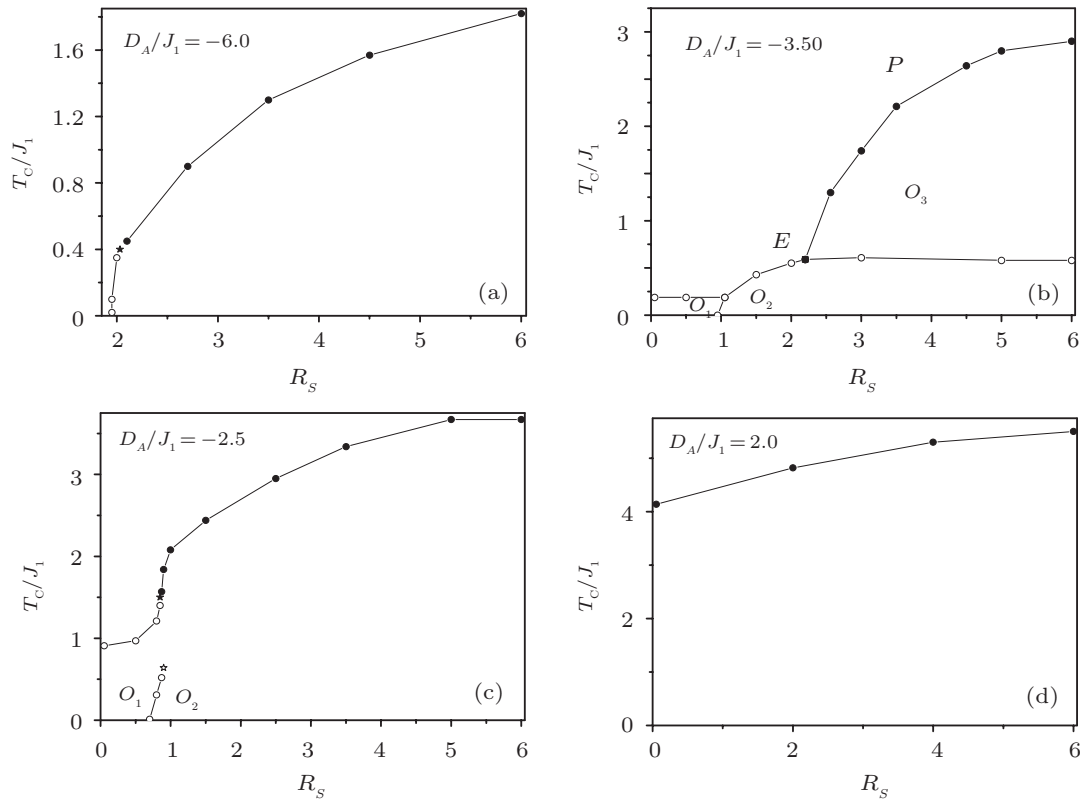


Fig. 4. The phase diagram of the system in the $(T/J_1, R_S)$ plane for $D_B/J_1 = -3.85$ and for $D_A/J_1 = -6.0$ (a), $D_A/J_1 = -3.5$ (b), $D_A/J_1 = -2.5$ (c), and $D_A/J_1 = 2.0$ (d).

ordered phases O_1 and O_2. This line is connected to a second first-order line at $R_S = 1.05$ and $T_C/J_1 = 0.19$, for $R_S \leq 1.05$ this second line separates the ordered phase O_1 from the disordered one P with a constant transition temperature $T_C/J_1 = 0.19$, while when $1.05 < R_S \leq 2.2$, it separates the ordered phase O_2 from the disordered one P with increasing critical temperature and it arrived at a triple point (E), the coordinates of which are ($R_S = 2.2$, $T_C/J_1 = 0.59$), from the triple point (E) when $R_S \geq 2.2$, this line separates the two ordered phases O_2 and O_3 with a constant critical temperature ($T_C/J_1 = 0.59$). The third line, which is of the second order, separates the ordered phase O_3 from the disordered one P, this line is obtained for $R_S \geq 2.2$ and it emerges from the triple point (E) with a critical temperature which increases to reach a saturation value ($T_{Csat}/J_1 = 2.9$) at high values of R_S. The third type of phase diagram is obtained for $-3.1 < D_A/J_1 < -2.0$, it is presented in Fig. 4(c), for $D_A/J_1 = -2.5$. In this phase diagram, we have three transition lines, the first one, in the low temperature region, is of the first order separating the two ordered phases (O_1, O_2). It starts from $R_S = 0.7$ at $T_C/J_1 = 0.0$ and increases speedily with R_S to terminate at an isolated critical point, which has coordinates ($R_S = 0.9$, $T_C/J_1 = 0.64$). The second one is of the first order too, separating the ordered and the disordered phases. It is clear that the critical temperature remains constant ($T_C/J_1 = 0.97$) below a threshold value of R_S which is equal to 0.5 and then increases with R_S to terminate at a tricritical point, from which a third second-order transition line starts and extends to reach a saturation value for large positive values of R_S. The fourth type obtained for $D_A/J_1 \geq -2.0$ is plotted in Fig. 4(d), as can be seen, the phase diagram contains almost second order phase transition line separating ordered and disordered phases. The explanation of the existence of the three ordered phases can be easily found in the crystal fields and the surface coupling reliance of M_A and M_B, since they are just related to the spin states of A- and B-atoms, for example, for $D_A/J_1 = -3.5$ and $D_B/J_1 = -3.85$, the phases O_1, O_2, and O_3 are characterized by ($M_A = 0.99$, $M_B = 0.60$) at $T_C/J_1 = 0.1$ for $R_S = 0.5$, ($M_A = 1.45$, $M_B = 0.84$) at $T_C/J_1 = 0.4$ for $R_S = 2.0$ and ($M_A = 0.29$, $M_B = 0.17$) at $T_C/J_1 = 1.0$ for $R_S = 3.0$, respectively.

To examine the influence of the uniaxial anisotropies on the phase diagrams of the system, we have plotted the variations of the critical temperature versus the uniaxial anisotropies D_A/J_1 (Fig. 5) and D_B/J_1 (Fig. 6) for $R_S = 0.05$ and for different values of D_B/J_1 and D_A/J_1, respectively. It is observed that the phase diagrams are very rich; they exhibit the first- and second-order transitions, the tricritical and the reentrant behaviors. In Fig. 5, depending on the value of D_B/J_1, we have two types of phase diagrams, in the first type, obtained for $D_B/J_1 \geq -2.0$, the system behaves like the spin-3/2 Blume–Capel model which does not exhibit a tricritical behavior;[31] the phase diagram exhibits a second-order transition line, separating the ordered and the disordered phases, it is clear that, the critical temperature remains constant ($T_C/J_1 = 1.85$ and 2.35 for $D_B/J_1 = 0.0$ and 6.0 respectively) below a threshold value of D_A/J_1 which depends on the value of D_B/J_1 ($D_{AC}/J_1 = -7.0$ and -8.0 for $D_B/J_1 = 0.0$ and 6.0 respectively) and then increases with D_A/J_1 to reach a saturation value which depends on the value of D_B/J_1 ($T_{Csat}/J_1 = 5.46$ and 5.95 for $D_B/J_1 = 0.0$ and 6.0 respectively). In the second type, obtained for $D_B/J_1 < -2.0$, we have a first-order transition line which starts, at $T_C/J_1 = 0.0$, from a value of D_A/J_1 which depends on D_A/J_1 (for example, for $D_B/J_1 = -3.85$, the value of D_A/J_1 is equal to -4.0), and it extends to terminate at a tricritical point, from this point a second-order transition line emerges and increases to reach a saturation value which depends also on the value of D_B/J_1 (for example, for $D_B/J_1 = -3.85$, $T_{Csat}/J_1 = 4.8$).

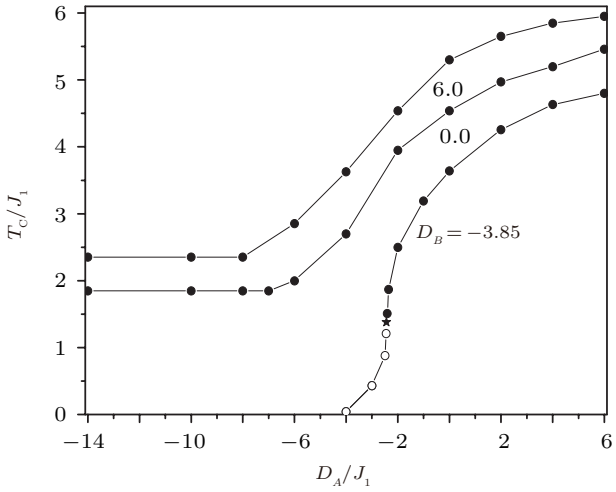


Fig. 5. The phase diagram of the system in the (T/J_1, D_A/J_1) plane for $R_S = 0.05$ and for different values of D_B/J_1.

In Fig. 6, the phase diagrams in the (D_B/J_1, T_C/J_1) plane are shown for selected values of D_A/J_1. For $D_A/J_1 = -6.0$, the phase diagram shows only a second-order phase transition, which starts from $D_B/J_1 = -2.01$ at $T/J_1 = 0.0$ and extends to reach a saturation value for large positive values of D_B/J_1. The system exhibits also the reentrant phenomenon, that is we have two successive second-order transition temperatures (for example for $D_B/J_1 = -2.25$, we have $T_C/J_1 = 0.18$ and 1.2), a similar behavior has been found in Refs. [32] and [33]. For $D_A/J_1 = -3.5$ and 0.0, in the phase diagram we have two lines separating the ordered and the disordered phases, one of the second-order for higher temperatures and the other of the first-order for lower temperatures which meet at a tricritical point. Increasing the value of the crystal field (D_A/J_1),

the coordinates of the tricritical point move to lower temperatures ($T_C/J_1 = 1.04$ for $D_A/J_1 = -3.5$ and $T_C/J_1 = 0.34$ for $D_A/J_1 = 0.0$). A reentrant phenomenon is also found for $D_A/J_1 = 0.0$ (for example for $D_B/J_1 = -6.05$, we have $T_C/J_1 = 0.24$, which is of a first order and $T_C/J_1 = 2.36$, which is of a second order). It is important to mention that, the reentrant phenomenon, in our case, results from the competition between the crystal fields D_A and D_B and the surface coupling interaction J_S.

In order to confirm the existence of the re-entrant phenomenon, which appears in Fig. 6, we have plotted the magnetization (Figs. 7(a) and 8(a)), the internal energy (Figs. 7(b) and 8(b)), and the susceptibility (Figs. 7(c) and 8(c)) dependencies on the temperature for $R_S = 0.05$, $D_A/J_1 = -6.0$, 0.0, and $D_B/J_1 = -2.4$, -6.05, respectively. We can see that, as the temperature is increased, the system passes from the paramagnetic (P) phase to the ordered phase and back to the P phase again, continuously as shows the internal energy curve (Fig. 7(b)), while it passes from the P phase to an ordered phase discontinuously and back to the P phase again continuously as is shown by the internal energy curve (Fig. 8(b)). Concerning the susceptibility curves, we observe that we have two peaks, for each figure, which coincide with the two successive transition temperatures.

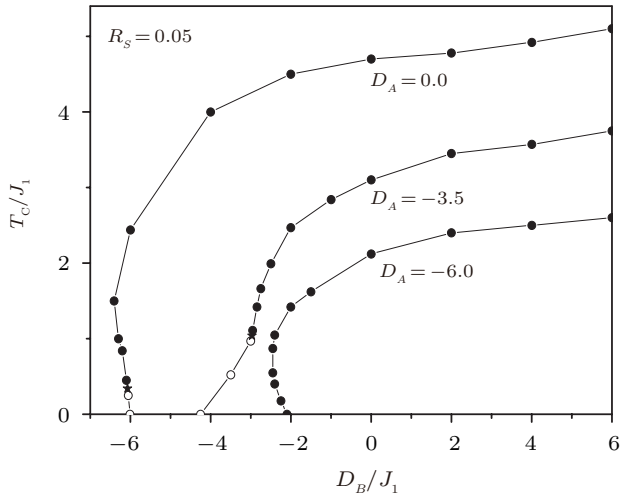


Fig. 6. The phase diagram of the system in the (T/J_1, D_B/J_1) plane for $R_S = 0.05$ and for different values of D_A/J_1.

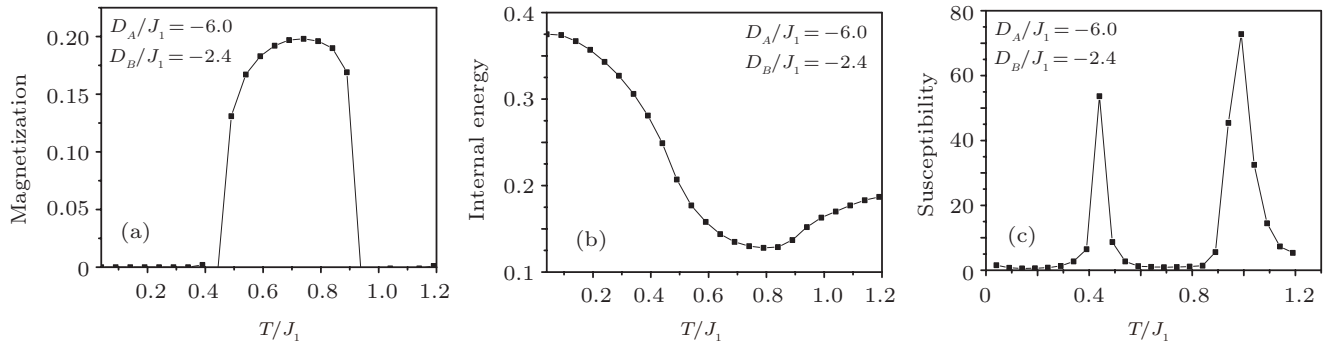


Fig. 7. Total magnetization (a), internal energy (b), and susceptibility (c) *versus* the temperature for $R_S = 0.05$, $D_A/J_1 = -6.0$, and $D_B/J_1 = -2.4$.

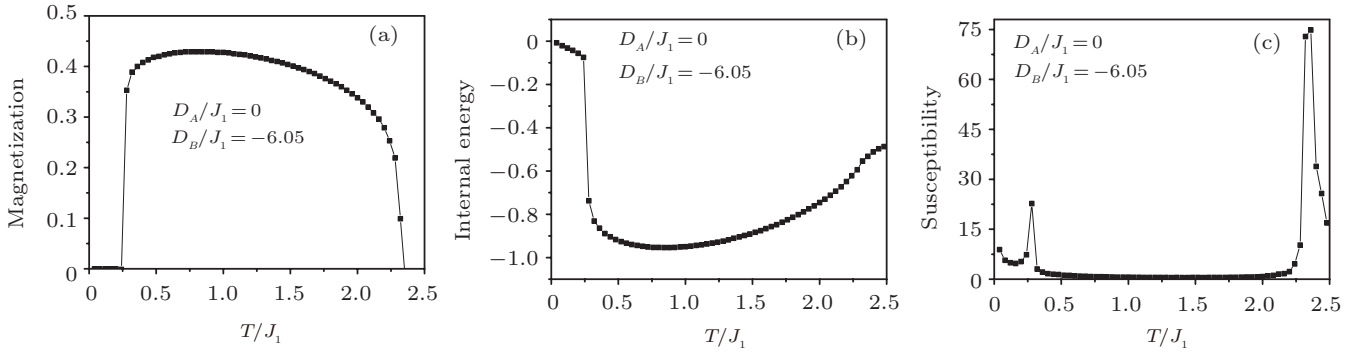


Fig. 8. Total magnetization (a), internal energy (b), and susceptibility (c) *versus* the temperature for $R_S = 0.05$, $D_A/J_1 = 0.0$, and $D_B/J_1 = -6.05$.

4. Conclusion

In conclusion, we have studied the magnetic properties and the phase diagrams of a ferromagnetic thin film system with different single-ion anisotropies acting on the spin-1 and the spin-3/2 by using the Monte Carlo simulation. We have discussed the influence of the uniaxial anisotropies and the surface coupling constants on the critical behavior. We have found that the system presents rich critical behaviors, which include the first- and the second-order transitions. It is shown that, depending on the values of the Hamiltonian parameters, the system can exhibit the tricritical, the isolated critical, and the critical end points. The possibility of obtaining a reentrant phenomenon has been highlighted.

References

[1] Sun X W, Jia C H, Liu X S, Li G Q and Zhang W F 2018 *Chin. Phys. B* **27** 047304
[2] Di Y N, Xu X M, Zhou J J and Doi M 2018 *Chin. Phys. B* **27** 024501
[3] Zhao B, Hu W, Tang X S, Huo W X, Han L L, Zhao M L, Ma Z G, Wang W X, Jia H Q and Chen H 2018 *Chin. Phys. B* **27** 047803 2018 *Chin. Phys. B* **27** 047803
[4] Wang Z, Xiao R Z, Zou C W, Xie W, Tian C X, Xue S W, Liu G A, Devi N and Fu D J 2018 *Chin. Phys. B* **27** 047901
[5] Zhang Y, Xu J, Zhou D Y, Wang H H, Lu W Q and Choi C K 2018 *Chin. Phys. B* **27** 048103
[6] Elmers H J 1995 *Int. J. Mod. Phys. B* **9** 3115
[7] Jiang Q and Tao Y M 2005 *Phys. Lett. A* **336** 216
[8] Charilaou M and Hellman F 2013 *Phys. Rev. B* **87** 184433
[9] Magoussi H, Boughazi B and Kerouad M 2018 *J. Supercond. Nov. Magn.* **31** 3817
[10] Kaneyoshi T 2014 *Physica B* **436** 208
[11] Kaneyoshi T 2014 *Physica E* **59** 50
[12] Kaneyoshi T 2013 *Physica E* **53** 14
[13] Kaneyoshi T 2013 *Physica B* **408** 126
[14] Kaneyoshi T 2013 *Physica B* **414** 72
[15] Boughazi B, Boughrara M and Kerouad M 2014 *Physica A* **401** 308
[16] ElAouad N, Moutie A and Kerouad M 2001 *J. Magn. Magn. Mater.* **233** 236
[17] Boughazi B, Boughrara M and Kerouad M 2017 *Physica A* **465** 628
[18] Boughazi B, Boughrara M and Kerouad M 2014 *Physica A* **401** 308
[19] Jie L W, Hua X Z, Lun C S and Chin Z C 2013 *Physics B* **22** 027501
[20] Yüksel Y 2014 *Physica B* **433** 96
[21] Ran C, Jin C and Roberts M 1988 *J. Appl. Phys.* **63** 3667
[22] Polak M, Rubinovich L and Deng J 1995 *Phys. Rev. Lett.* **74** 4059
[23] Tang H 1985 *Phys. Rev. Lett.* **71** 444
[24] Boughrara M, Kerouad M and Zaim A 2016 *J. Magn. Magn. Mater.* **410** 218
[25] Stanica N, Stager C V, Cimpoesu M and Andruh M 1998 *Polyhedron* **17** 1787
[26] Abubrig O F, Horvath D, Bobak A and Jascur M 2001 *Physica A* **296** 437
[27] Souza I J, de Arruda P H Z, Godoy M, Craco L and de Arruda A S 2016 *Physica A* **444** 589
[28] Landau D P and Binder K 2004 *A Guide to Monte Carlo Simulations in Statistical Physics* (Cambridge: Cambridge University Press)
[29] Feng Y Q, Jin K J, Ge C, He X, Gu L, Yang Z Z, Guo H Z, Wan Q, He M, Lu H B and Yang G Z 2016 *Chin. Phys. Lett.* **33** 076801
[30] Urushibara A, Moritomo Y, Arima T, Asamitsu A, Kido G and Tokura Y 1995 *Phys. Rev. B* **51** 14103
[31] Štubňa V and Jaščur M 2017 *J. Magn. Magn. Mater.* **442** 364
[32] Keskin M and Ertaş M 2018 *Physica A* **496** 79
[33] Costabile E, Viana J R, Sousa J R and de Arrudac A S 2015 *Solid State Commun.* **212** 30